Journal of Fluorescence (2019) 29:981–992
https://doi.org/10.1007/s10895-019-02411-2

ORIGINAL ARTICLE

Tryptophan / Dextran70 Based - Fluorescent Silver Nanoparticles: Synthesis and Physicochemical Properties

Mariana Voicescu[1] · Sorana Ionescu[2] · Jose M. Calderon-Moreno[1] · Valentin S. Teodorescu[3] · Mihai Anastasescu[1] · Daniela C. Culita[1]

Received: 2 May 2019 / Accepted: 2 July 2019 / Published online: 18 July 2019

Abstract

Nano-size and shape of fluorescent silver nanostructures are important for a wide range of bio-applications, especially as drug delivery systems, imaging and sensing. The aim of the work is to develop a fluorescent silver nano-structured system, synthesized by chemical reduction of aqueous $AgNO_3$ solution by Tryptophan using Dextran 70 as stabilizing agent ($SNPs^{FL}$). The formed fluorescent nano-system was analyzed by UV-Vis absorption, DLS, SEM, TEM, AFM, steady-state and time resolved fluorescence spectroscopy. TEM analysis showed multi-twined nanoparticle, with the size within 15–40 nm. $SNPs^{FL}$ shows the fluorescence emission at 346 nm, the fluorescence quantum yield, $\Phi = 0.034$ and the integrated fluorescence lifetime, $<\tau> = 1.82$ ns. Riboflavin fluorescence behaviour in the RF/$SNPs^{FL}$ system, has been also studied. The results have relevance in using $SNPs^{FL}$ as a potential marker/emissive system to solve various biological barriers in humans, like drug release and protein structure.

Keywords Fluorescence spectroscopy · Silver nanoparticles · Tryptophan · Riboflavin

Introduction

Nanoscience by the commercially and synthesized nano-sized materials play an important role in biology and medicine, and is currently employed as a tool to explore several problems especially regarding gene and drugs delivery systems [1, 2]. In this context, pharmaceutical sciences are using nanoparticles to reduce toxicity and the side effects of drugs, but the risks imposed by the carrier systems is still not very well understood [3].

Among nano-sized materials, silver nanoparticles (SNPs) are being used as a medium to transport and release several drugs [4, 5] and in antibacterial, antimicrobial and disinfecting formulations [6–10]. The size, shape and composition of SNPs play an important role on their efficacy and related to this issue synthesis and optical properties of SNPs [11, 12], focused on their fluorescence characteristics, have been reported [13–18]. According to Zheng and Dickson, 2002, silver clusters formed by photo-reduction of silver ions in the dendrimer host (1:12 dendrimer: Ag) have strong fluorescence, while the larger NPs formed through reduction with $NaBH_4$ were non-fluorescent [16]. It was found that fluorescence grows with increasing irradiation time as silver ions are photo-reduced, within ~6 s, the field of view being filled with individual blinking fluorescent species, with little subsequent photo-activation [16]. Jacob et al. 2011, studied the formation of SNPs by the reduction of $AgNO_3$ using tryptophan (Trp) under alkaline conditions, and showed that the replacement of BH_4^- ions adsorbed on the nanoparticle surface by Trp destabilizes the particles and further causes aggregation [19].

Based on fluorescence quenching, fluorescent silver nanoparticles [20–23] were used for the selective and highly sensitive detection of Pb(II), at 200 ppq level [24], of S^{2-} with a detection limit of 2 nM [25]. They were used as well for their toxicological effect in aquatic environments (Goldfish) and human hepatoma cells (HepG2) [26]. Regarding in vivo studies on oxidative stress, photosynthesized emissive SNPs

✉ Mariana Voicescu
voicescu@icf.ro

[1] Institute of Physical Chemistry "Ilie Murgulescu" of the Romanian Academy, Splaiul Independentei 202, 060021 Bucharest, Romania

[2] Department of Physical Chemistry, University of Bucharest, Bd. Regina Elisabeta 4-12, 030018 Bucharest, Romania

[3] Institute of Atomic Physics, National Institute of Materials Physics, 077125 Magurele, Romania

containing as organic dye the 2-amino-anthracene, caused larger changes in livers than in intestines with Glutathione-S-Transferase (GST) level measurements, suggesting the importance of NPs size in terms of its toxicity while for in vivo studies in HepG2 cancer cells, a less toxicity by cell viability measurements, were observed [26].

Recently, it was reported that Trp-stabilized SNPs, possess antitumor activity and exhibit lower pro-oxidant activity in relation to cellular lipids, but do not differ from the SDS-stabilized NPs in their ability to induce protein oxidation [27]. Thus, the use of Trp in NPs synthesis is effective in attenuating the potential hepatotoxicity and nephrotoxicity of NPs during their in vivo application [27].

The aim of the present work is to develop a fluorescent silver nano-structured system, synthesized by chemical reduction of aqueous $AgNO_3$ solution by Tryptophan using Dextran 70 as stabilizing agent ($SNPs^{FL}$). TEM analysis showed that the formed nanostructures are multi-twined nanoparticles, with the size within 15–40 nm. The surface plasmon resonance peak of $SNPs^{FL}$ shows maximum absorption at 463 nm with the fluorescence emission at 346 nm and the fluorescence quantum yield, $\Phi = 0.034$ and the integrated fluorescence lifetime, $<\tau> = 1.82$ nm. Riboflavin fluorescence behaviour in the RF / $SNPs^{FL}$ system, has been also studied. The results support the idea of using it as a potential marker/emissive system to solve various biological barriers in humans, like drug delivery and protein structure.

Experimental

Materials

Synthesis of fluorescent silver nanoparticles: ($SNPs^{FL}$) were prepared by chemical reduction. The silver nitrate ($AgNO_3$, ≥ 99%, purchased from Sigma-Aldrich) of 0.02 M and the blend of reducing agents, Tryptophan (L-Trp, ≥ 98%, purchased from Sigma Aldrich) of 8 mM and Dextran 70 (Dx70, purchased from ROTH) of 1.2%, Dx70 being a stabilizer too, were stirred at room temperature, at 700 rpm. The colorless initial solution turned to pale yellow towards pale pink after aprox. 30 min of stirring while, after 1 h of continuous stirring the color of the solution became open brick toward reddish, which indicates the formation of $SNPs^{FL}$. The solution is clear and the color open brick toward reddish is kept during 1 week at room temperature.

For DLS and TEM analysis, 500 μl of $SNPs^{FL}$ solution were centrifuged at 7000 rpm, 5 min for purification and the sediment was washed twice with distilled water.

Riboflavin (RF) was purchased from Fluka and aliquots from a stock aqueous solution of 0.2 mM were used such that the final working concentration was of 3×10^{-5} M.

Methods

UV-Vis Absorption measurements were recorded using a Perkin Elmer, Lambda 35, UV-Vis Spectrometer, the scan rate of 480 nm/min and the spectral resolution of 1 nm. The concentration of $SNPs^{FL}$ was estimated using the Beer-Lamber law with the relationship between molar extinction coefficient and diameter, according to Navarro and Werts, 2013 [28].

Dynamic Light Scattering (DLS) measurements for the average hydrodynamic size of the particles dispersed in water was performed with a Beckman Coulter Delsa Nano C particle analyzer (Brea, CA, USA). Zeta potential was measured by Electrophoretic Light Scattering, using the same equipment.

Scanning electron microscopy (SEM) was performed with a high-resolution FEI Quanta 3D FEG microscope operating at an acceleration voltage of 10 kV, using an Everhart–Thornley secondary electrons (SE) detector. Drops of the as prepared silver nanoparticles solution were deposited on a Si substrate and observed by SEM after evaporation of the liquid part at room temperature. A second sample was subjected to

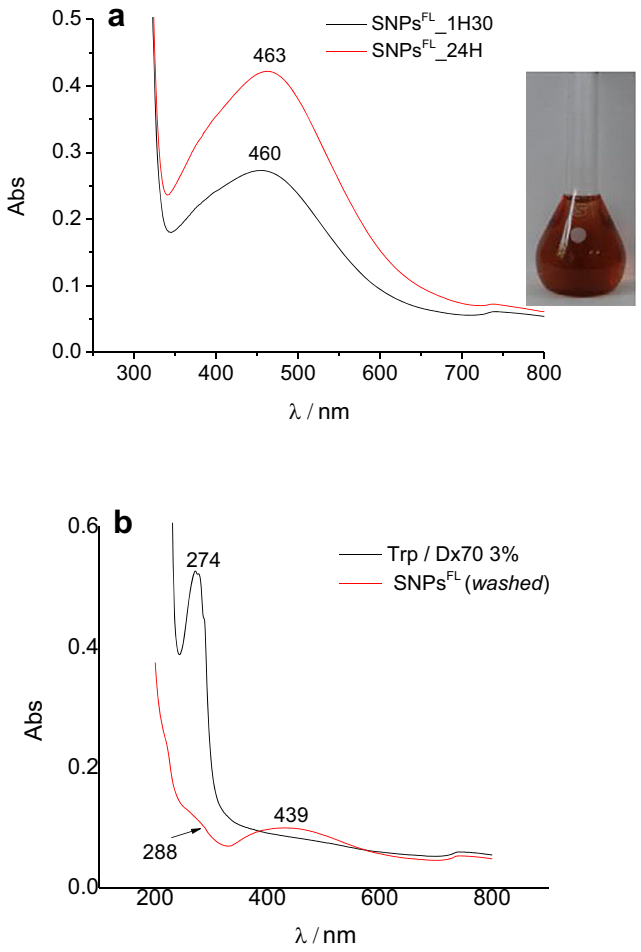

Fig. 1 UV-visible absorption spectrum of $SNPs^{FL}$; *The inset* picture showing the color of $SNPs^{FL}$(**a**) and the absorption spectrum of the washed $SNPs^{FL}$ and Trp; [Trp] = 3×10^{-5} M (**b**)

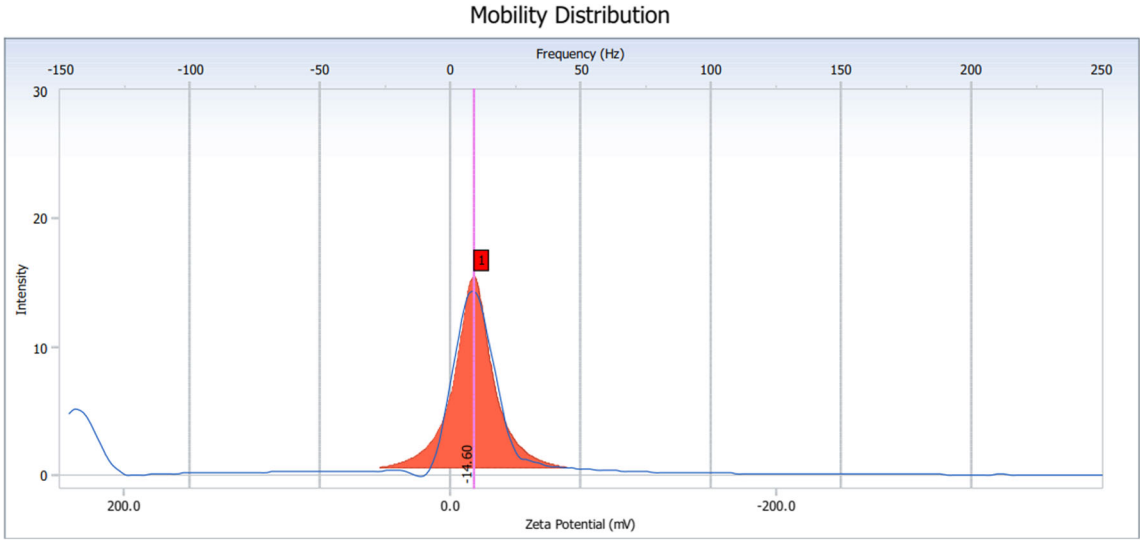

Fig. 2 Volume distribution and zeta potential profile of $SNPs^{FL}$

rapid thermal annealing (RTA): heated at a rate of 10 °C/min up to 160 °C, this temperature was held for 5 min and the sample cooled down before observation.

Transmission Electron Microscopy (TEM) analysis was taken using a transmission electron microscope model JEM 200CX equipped with a KeenView CCD camera and operating at 120 kV.

Atomic Force Microscopy (AFM) measurements were undertaken with XE-100 microscope from Park Systems, in true non-contact™ mode - the working mode

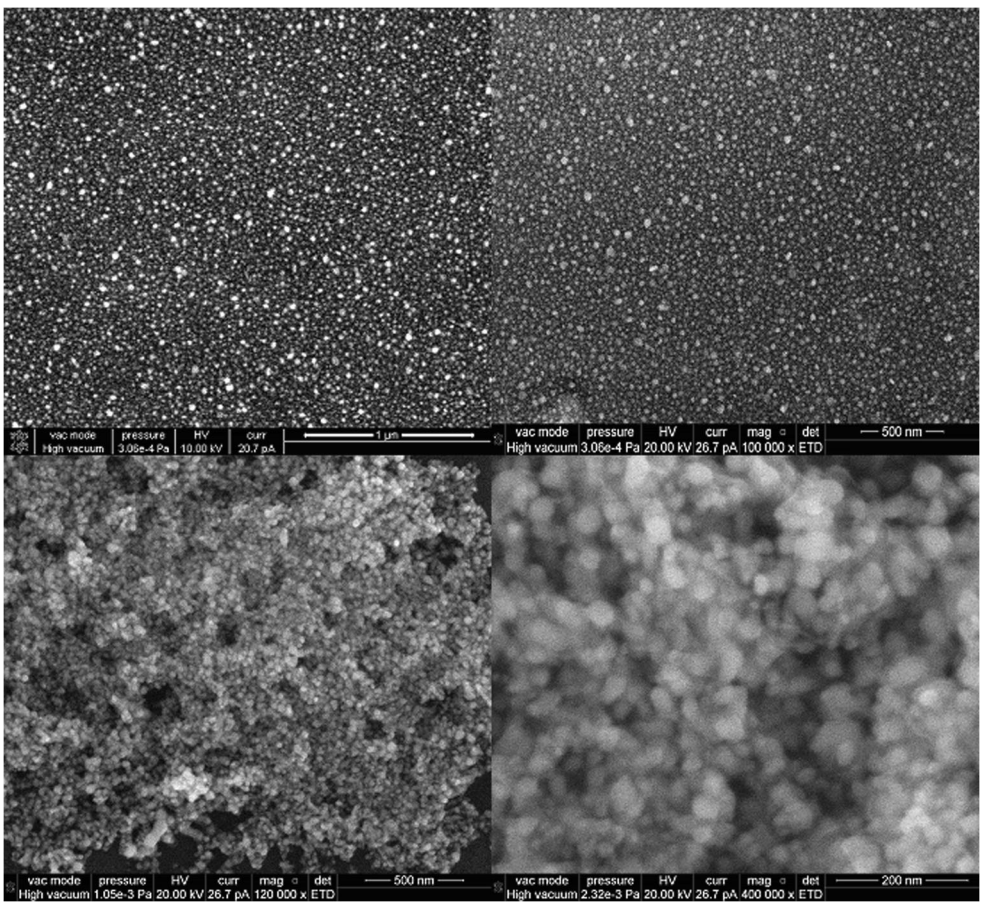

Fig. 3 SEM micrographs of $SNPs^{FL}$ after deposition (top) and after RTA (bottom)

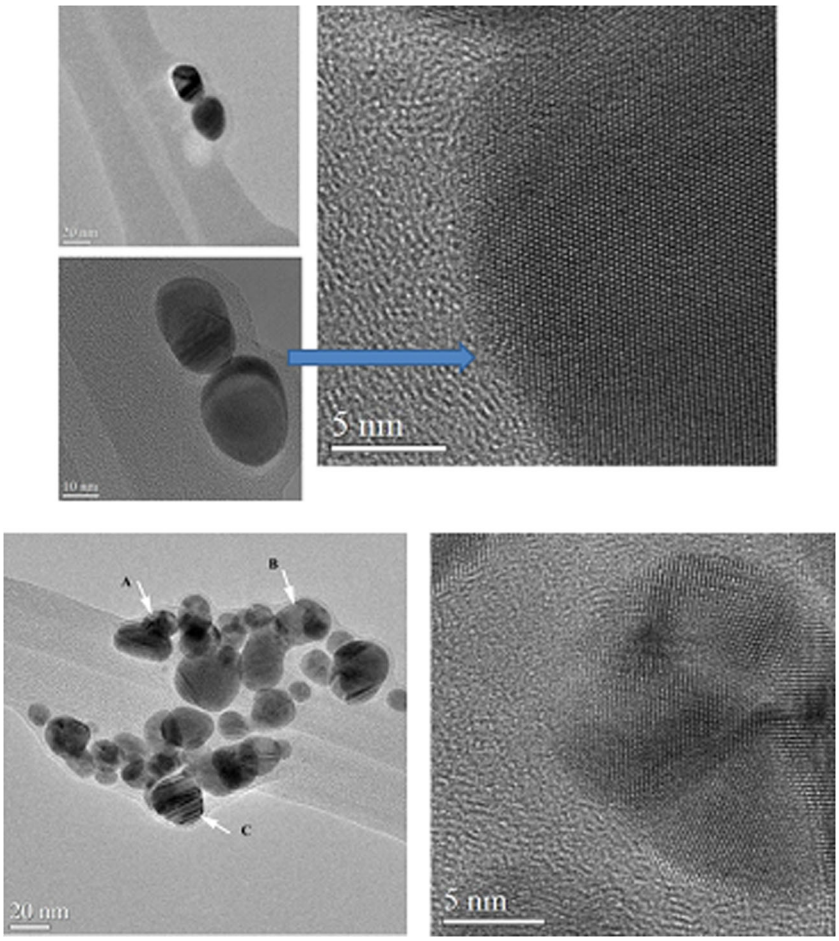

Fig. 4 TEM micrographs at different magnifications of $SNPs^{FL}$

recommended for soft samples. The scanner of the XE100 apparatus is equipped with flexure-guided, cross talk eliminated scanners, thus allowing the imaging of very small objects at the nanometric scale. All AFM images have been recorded with sharp tips (<8 nm tip apex), NCHR type from Nanosensors™, of *aprox*. 125 μm length, 30 μm width, spring constant 42 N/m, and 330 kHz resonance frequency. For the AFM experiments, a small quantity of $SNPs^{FL}$ variant was deposited on high quality quartz pieces and dried at room temperature. The recorded AFM images were processed with XEI program (v 1.8.0 - Park Systems) for displaying purpose.

Fluorescence emission and excitation spectra were recorded with a Jasco FP-6500 Spectrofluorometer, using 3–5 nm bandpass for the excitation and the emission monochromators, the detector response of 1 s, data pitch of 1 nm, the scanning speed of 100 nm/min. The excitation wavelength was 295 nm (for Trp emission).

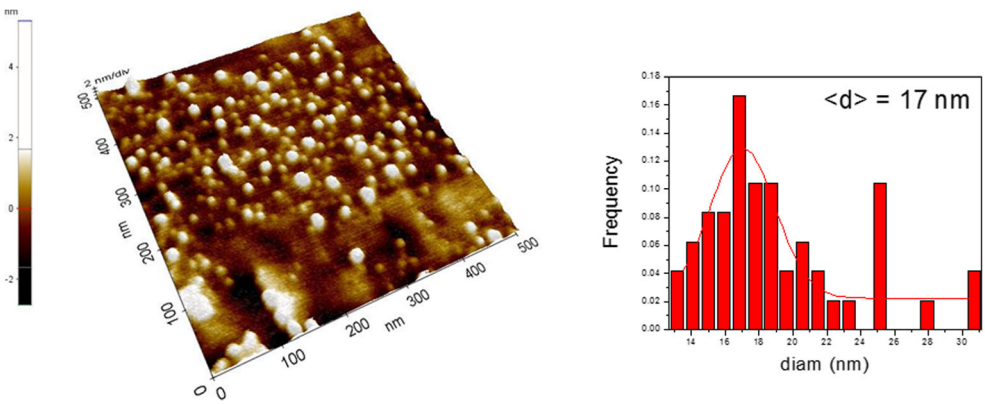

Fig. 5 2-D AFM image with the size distribution of $SNPs^{FL}$

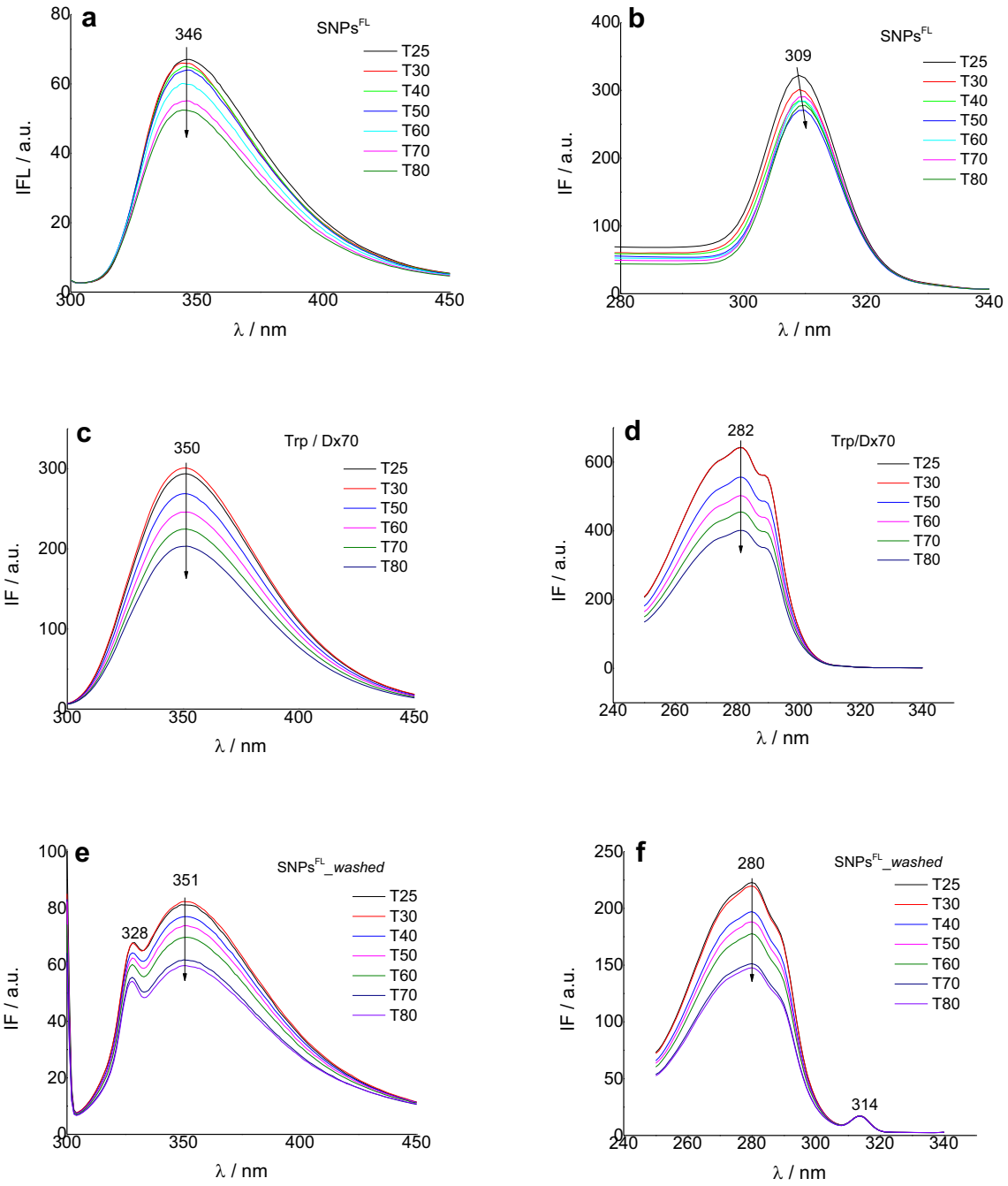

Fig. 6 Temperature effect on the fluorescence emission (*left*) and excitation (*right*) spectra of $SNPs^{FL}$, Trp/Dx70 and washed $SNPs^{FL}$; $\lambda_{ex} = 295$ nm; $\lambda_{em} = 350$ nm; $[Trp] = 3 \times 10^{-5}$ M; [Dx70] = 3%

To determine the fluorescence quantum yields for synthesized fluorescent silver nanoparticle, the following equation has been used, with Trp as emission standard:

$$\Phi_{SNPs} = \left(F_{SNPs} \times A_{Trp} \times \Phi_{Trp}\right) / F_{Trp} \times A_{SNPs} \quad (1)$$

where, Φ_{Trp} is the known quantum yield of Trp in water, Φ = 0.13 [29], F_{SNPs} and F_{Trp}, are the integrated fluorescence intensities of the silver nanoparticles and Trp reference, A_{Trp} and A_{SNPs} are the absorbance of the reference and the silver nanoparticles, with F_{Trp} and A_{Trp} in Dx70 3% aqueous solution.

The Excitation-Emission Matrix (EEM) spectra were recorded by scanning the excitation wavelength in the range of 250–520 nm with a step of 10 nm and measuring the emission spectrum. Contour plots were then constructed with the dedicated software provided by the manufacturer. They contain scattering data as well ($\lambda_{ex} = \lambda_{em}$), which should be disregarded.

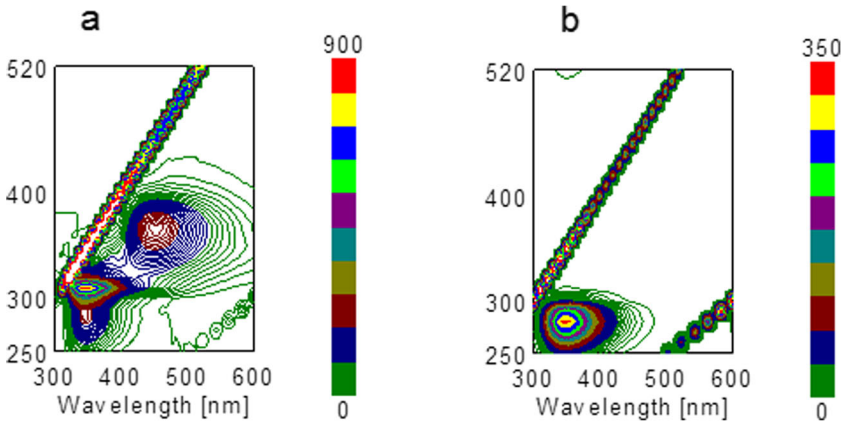

Fig. 7 Contours of the excitation-emission matrix measurements for the prepared SNPs^{FL} (**a**) and Trp/Dx70 (**b**) (x/y-emission/excitation wavelength in nm, intensity in a.u.)

The fluorescence lifetime decays were recorded in a time-correlated single photon counting FLS920 system from Edinburgh Instruments, with led excitation at 294.5 nm and laser excitation at 375.6 nm, a lifetime scale of 50 ns and 2048 channels. The instrument response function was measured on a scattering ludox sample. The data were fitted as bi-exponential decays and the goodness of fit was checked on grounds of χ^2; when values exceeded 1.2 a third component was added. Intensity-averaged lifetimes were calculated according to the eq. (2); the fractional emission intensity of the *i*th component is defined as the eq. (3):

$$\langle \tau \rangle = \frac{\sum_i \alpha_i \cdot \tau_i^2}{\sum_i \alpha_i \cdot \tau_i} \tag{2}$$

$$f_i = \frac{\alpha_i \cdot \tau_i}{\sum_i \alpha_i \cdot \tau_i} \tag{3}$$

Results and Discussion

UV-vis Analysis

The surface plasmon resonance band observed the in UV-visible absorption spectrum of SNPs^{FL} at two stages of reduction of silver ions, at 24H (λ_{abs} = 460 nm) and 1H30, (λ_{abs} = 463 nm) to SNPs^{FL}, indicated the formation of colloidal silver nanoparticles, Fig. 1a. A shoulder at ~ 387 nm in the absorption bands is attributed to the formed spherical small NPs [30, 31].After 1H30 min, an increase in the absorption intensity with 3 nm batochormic shifted of the plasmon band indicates that NPs partially aggregates to form clusters/larger agglomerates. The reduction of silver ions ($Ag^+ \rightarrow Ag^0$) was visible evident from colourless (initially) - yellow pale (after 30 min) up to brick - reddish, after the process of reduction, Fig.1a – ***inset***. The concentration of SNPs^{FL} was found to be 0.0132 nM, and they showed no changes in the absorption spectra even after one week of ageing time.

To check the Trp profile, Fig. 1b shows by the position of the surface plasmon band of the washed NPs. A blue-shift of 24 nm, λ_{max} ~ 439 nm, of the surface plasmon band with the Trp slightly absorption band at ~ 288 nm, is noticed. As can be observed, λ_{max} value of Trp in Dx70 was found to be 274 nm, Fig. 1b. The red-shift of the present Trp may be attributed to differences in the surface environment. Therefore, the Trp linkage by hydrophobic interaction to the NPs surface as well as a conjugation of the formed NPs around un-interacted Trp, has occurred. Also, the variation in the absorption intensity, the decrease in plasmon band with the increase of the 288 nm absorption band may suggest the presence of two Trp conformers in the SNPs complex.

DLS Analysis

DLS analysis of the SNPs^{FL} revealed an average size of 135.7 nm and a good polydispersity index, PDI = 0.310, thus the presence of mono-dispersed particles. The mobility

Table 1 Fluorescence lifetime measurements parameters: α_i-pre-exponential factor, %, f_i fractional emission intensity, %, τ_i-fluorescence lifetime, $<\tau>$ −intensity-averaged lifetime (lifetimes in ns)

System	λ_{em} / nm	α_1	α_2	α_3	f_1	f_2	f_3	τ_1	τ_2	τ_3	$<\tau>$
λ_{ex} = *294.6 nm*											
SNPs^{FL} *as prepared*	350	54.07	45.69	0.24	25.13	67.27	7.591	0.241	0.762	16.383	1.82
SNPs^{FL} *washed*	350	76.00	23.22	0.78	43.82	44.1	12.08	0.296	0.996	7.947	1.52
Trp/Dx70	350	74.74	23.16	2.11	39.21	47.37	13.42	0.502	1.979	6.554	2.06

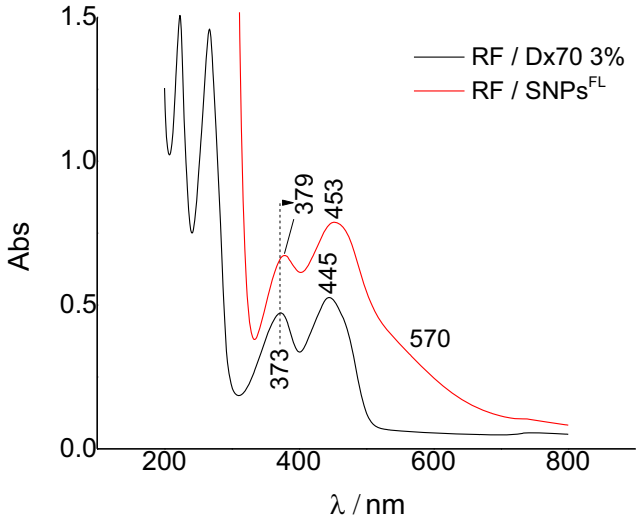

Fig. 8 UV-Vis absorption spectrum of RF in $SNPs^{FL}$ and Dx70 3% systems

(-1.138×10^{-4} cm^2/Vs) distribution exhibited a zeta potential $\zeta = -14.60$ mV, Fig. 2. This value provides a good physical stability of $SNPs^{FL}$ with the tendency towards agglomeration; the presence of electric charges on the $SNPs^{FL}$ surface favours agglomeration. The efficiency of the Dx70 in stabilizing $SNPs^{FL}$ by providing negative charges that leads to particles agglomeration or formation of self assembled aggregates, is taken into consideration.

SEM Analysis

SEM analysis of the $SNPs^{FL}$ solution deposited in a Si substrate and dried at room temperature revealed the deposition of a layer of silver nanoparticles with diameters around 30 nm. After drying, the silver nanoparticles remain well dispersed in the highly stable organic stabilizer, Dextran70, solid at room temperature, up to *aprox.* 200 °C, Fig. 3 - ***top***. The sample treated by RTA, Fig. 3 - ***bottom***, showed more details in the size and shape of the stabilized nanoparticles, agglomerated after densification of the hybrid layer, the blurred appearance of the image is caused by the stabilizer coating the Ag nanocrystallites.

TEM Analysis

TEM micrographs at different magnifications of $SNPs^{FL}$ are shown in Fig. 4. Figure 4 - ***top*** shows independent particles with Ag nanocrystal in <111> facets as major planes. In Fig. 4 - ***bottom*** one can see that polycrystalline NPs are generated, that Ag nano-crystallites (A, B, C) full of defects are welded, twined and partially aggregate to form larger clusters. The average particle size of the measured particles was as small as 15–40 nm. For clarity sake, multi-twined nanoparticles at higher magnification are presented.

AFM Analysis

AFM analysis confirmed the nano-scaled $SNPs^{FL}$ and gave useful morphological details regarding their shapes and the size distribution, Fig. 5. Individual $SNPs^{FL}$ are spherical in shape and the size is ~ 17 nm, however aggregates of higher diameter are observed.

Fluorescence Analysis

Steady-State Fluorescence Measurements

Fluorescence emission spectra of $SNPs^{FL}$ exhibit a single emission peak with maximum centered at 346 nm, feature due to Trp fluorescence. The found fluorescence quantum yield of $SNPs^{FL}$ is 0.034. As temperature increases, 25–80 °C range, the fluorescence intensity of $SNPs^{FL}$ slowly decreases without shifts in emission wavelength, Fig. 6a. Its corresponding fluorescence excitation spectra show a maximum at 309 nm, due to the Trp deprotonated form at NPs surface, with slightly batochromic shifted as temperature increases, Fig.6b. Also, an extension of $\pi \rightarrow \pi^*$ transition, is considered [32].

In direct comparison, Trp fluorescence in Dx70, showed an emission peak at 350 nm and the fluorescence intensity gradually deceases as temperature increases and no emission shifts are noticed, Fig. 6c. Fluorescence excitation spectra show a maximum at 282 nm, appearing from $\pi \rightarrow \pi^*$ transition of the aromatic amino acid residues [32, 33] corresponding thus to Trp absorption, Fig. 6d.

Comparison of the $SNPs^{FL}$ before (Fig. 6a) and after Trp washing, (Fig. 6e) shows the appearance of two emission peaks with maximum at 328 nm and 351 nm, with a higher level of the fluorescence intensity. The 5 nm red-shifted, $\lambda_{em} = 351$ nm, corresponds to a more hydrophilic environment of Trp on NPs surface while the emission peak at 328 nm, appears from a buried Trp into $SNPs^{FL}$. Thus in washed $SNPs^{FL}$, an increase in Trp surface hydrophobicity takes place. Fluorescence excitation spectra, Fig. 6f, exhibits two maxima: at 280 nm, corresponding to Trp absorption and at 314 nm, attributed to the deprotonation of hydroxyl group with π-electrons delocalization at the NPs surface [33]. It is also observed that as temperature increases, the band at 280 nm slightly linearly decreases while, the band at 314 nm remains unchanged, Fig. 6f. The feature may suggest no

Scheme 1 RF reduction at the $SNPs^{FL}$ surface

$$SNPs^{FL} + RF \underset{-H^+}{\overset{+H^+}{\rightleftharpoons}} SNPs^{FL} - RF_{ox}H^+ \underset{-2H^-}{\overset{+2H^+}{\rightleftharpoons}} SNPs^{FL} - RF_{red}H_2$$

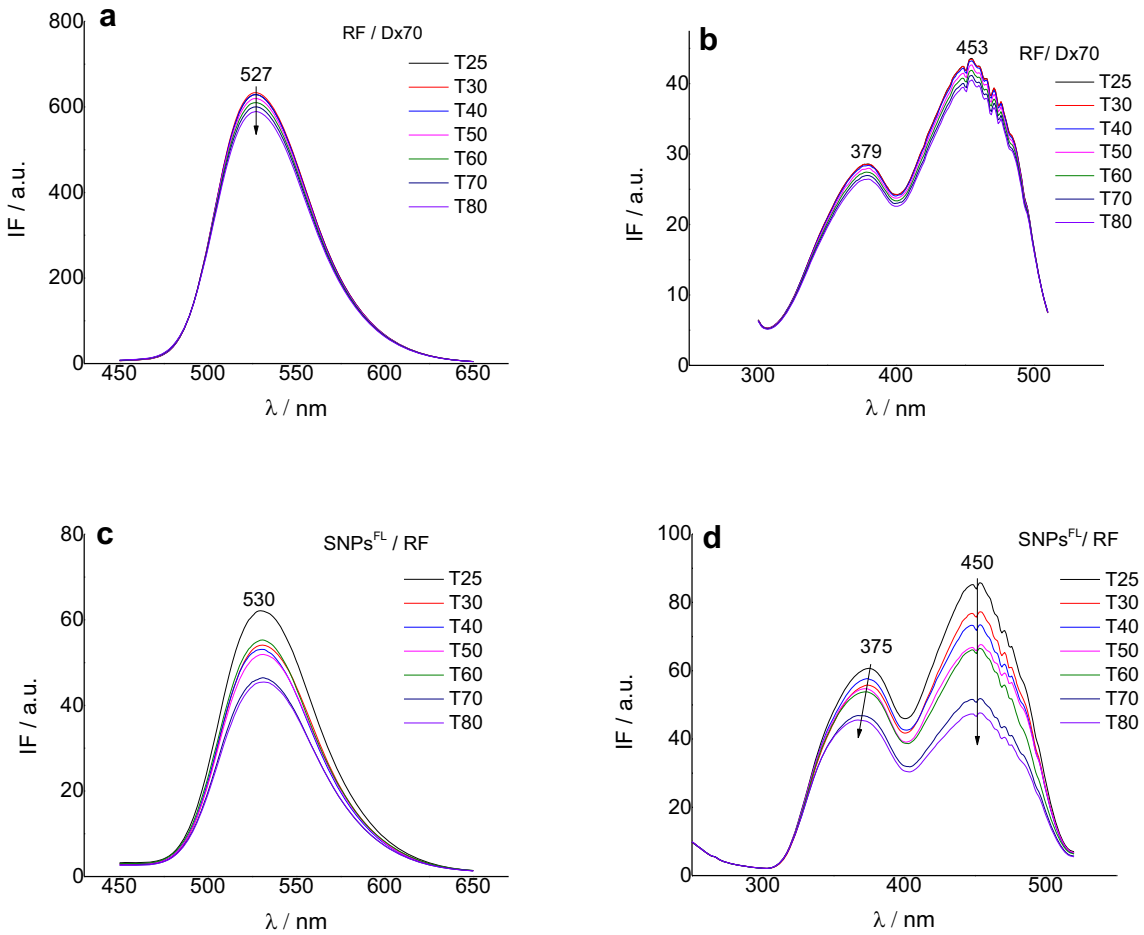

Fig. 9 Fluorescence emission (**ac**) with their corresponding excitation (**bd**) spectra *on the RF band* of the RF/Dx70 3% and SNPs^{FL}/RF systems, as a function of temperature; [RF] = 3×10^{-5} M; [Dx70] = 3%; λ_{ex} = 365 nm; λ_{em} = 520 nm

subsequent thermal destruction of Trp electronic structure, no changes in the Trp environment for both, the buried Trp and the Trp on the SNPs^{FL} surface.

Overall, fluorescence emission of the washed SNPs^{FL} appears from two Trp rotamers: one buried into SNPs^{FL} complex with λ_{em} = 328 nm and the other more exposed to the interactions on the NPs surface, with λ_{em} = 351 nm. Also, an increase in Trp surface hydrophobicity, as a good indication of protein containing Trp stability, is taken into consideration.

3D-Excitation-Emission Matrix Measurements

The 2D contours representing the projection of the excitation-emission matrix measurements in the wavelengths plane are presented in Fig. 7. The main band of the SNPs^{FL} (Fig. 7a) corresponds to Trp, with an excitation maximum at 286 nm and a spike at 308 nm (attributed to the Raman water band), while the emission maximum is at 350 nm. In direct comparison, from contour of Trp/Dx70 (Fig. 7b), it results that the band specific to Trp is found at the excitation and emission wavelength of 280 and 350 nm, respectively.

Lifetime Measurements

The resulting lifetime parameters are presented in Table 1. The prepared SNPs^{FL} have Trp as an intrinsic fluorophore. It was shown that Trp has two lifetime components in water [34, 35], with lifetimes of 3.1 and 0.53 ns at pH = 7. The presence of Dx70 in aqueous medium gives rise to a third component, with a longer lifetime of 6.55 ns, while the other two decrease to 1.98 and 0.50 ns, respectively. There is a further decrease of the shortest lived two Trp components for the sample that contain SNPs^{FL} to 0.24 and 0.76 ns, respectively, while the longest one increases up to 16.38 ns.

Riboflavin (RF) Fluorescence Behaviour into RF / SNPs^{FL} System

Absorption Measurements

As fluorescent and photosensitive probe able to easily interacts with several biological molecules with application in diagnoses [36–42], in order to see changes in the electronic

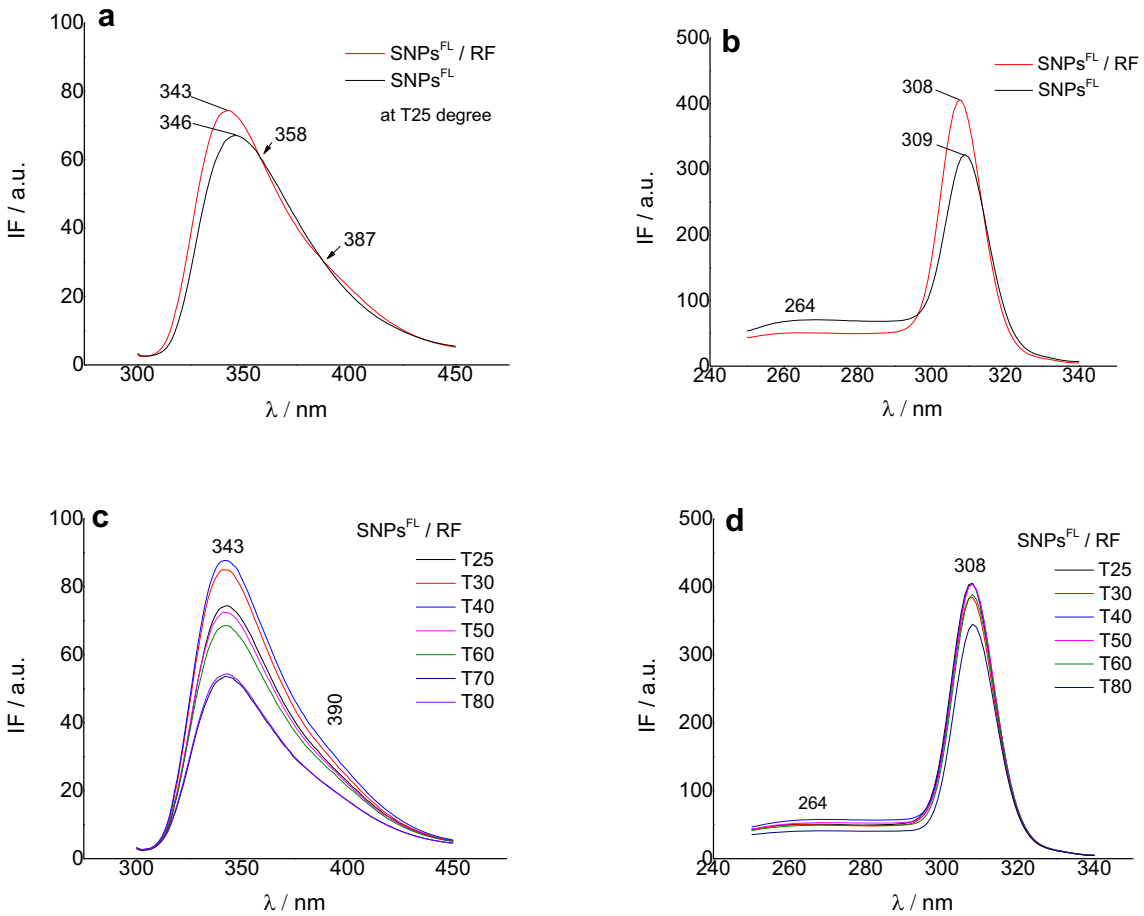

Fig. 10 Fluorescence emission (**ac**) with their corresponding excitation (**bd**) spectra *on the Trp band* of the SNPs^{FL} and SNPs^{FL}/RF systems, as a function of temperature; [RF] = 3 × 10^{-5} M
λ_{ex} = 295 nm; λ_{em} = 350 nm.

structure, Fig. 8 presents by comparison the absorption spectra of RF in the RF/SNPs^{FL} and RF/Dx70 systems. Two

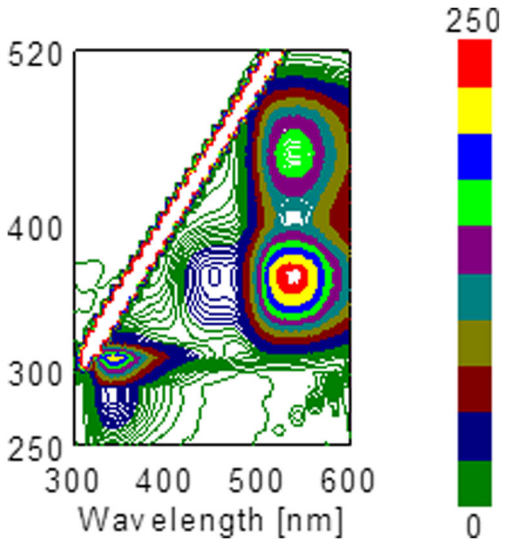

Fig. 11 Contour of the excitation-emission matrix measurements for the prepared SNPs^{FL} / RF system (x/y-emission/excitation wavelength in nm, intensity in a.u.)

absorption peaks at 379 and 453 nm (specific to $\pi \rightarrow \pi^*$ transition) with a broad absorption band at ~ 570 nm, were observed. The last one may be attributed to the reduced form of RF at the SNPs^{FL} surface, suggesting a hindering of the silver ion release leading in this way to a lower toxicity of the SNPs^{FL} [31].

Compared with RF/Dx70 system where λ_{abs} = 373/445 nm, in RF/SNPs^{FL} system, 6–8 nm batochromic shifts were observed (bands at λ_{abs} = 379/453 nm) and these could be due to the superimposition of the plasmonic band of SNPs or may suggest the Trp-RF interaction by H-bonds at the SNPs^{FL} surface. Also, changes in the absorption shape of RF with the decrease of the absorbance intensity occur, Fig.8 The possible reaction of RF reduction at the SNPs^{FL} surface may be described as follows, Scheme 1.

Steady-State and Time-Resolved Fluorescence Measurements

The influence of temperature (25–80 °C range) on the fluorescence behaviour of RF in Dx70 is shown in Fig. 9a. As temperature increases, the emission maximum at 527 nm remains

Table 2 Fluorescence lifetime measurements parameters: α_i-preexponential factor, %, f_i-fractional emission intensity, %, τ_i-fluorescence lifetime, $<\tau>$ −intensity-averaged lifetime (lifetimes in ns)

System	λ_{em} / nm	α_1	α_2	α_3	f_1	f_2	f_3	τ_1	τ_2	τ_3	$<\tau>$
λ_{ex} = 375.6 nm											
$SNPs^{FL}$ /RF	450	68.91	12.61	18.49	6.929	17.17	75.9	0.21	2.78	8.45	6.91
	530	–	56.86	43.14	–	45.23	54.77	–	2.41	3.84	3.19

unchanged and no significant RF fluorescence quenching is noticed. Also, no changes in the electronic structure of RF in the excited state, λ = 379/453 nm, are observed, Fig. 9b. In the $SNPs^{FL}$/RF system, the decrease of the fluorescence intensity of RF is ~ 10 times greater than that in Dx70 without changes in shape, Fig. 9c. The RF fluorescence emission is not significantly changed, 3 nm red-shifted towards λ_{em} = 530 nm and no emission shifts as temperature increases are noticed. The feature may suggest no aggregation, but rather a dissociation of RF molecule in the $SNPs^{FL}$/RF system. Fluorescence excitations spectra of RF in $SNPs^{FL}$/RF systems present two maxima at 375 and 450 nm, slight hypsochromic-shifted compared to RF in Dx70, Fig. 9 d. As temperature increases, the 375 nm band continues to be slight hypsochromic shifted while no shifts of the band at 450 nm are observed. Also, no changes in the shape are noticed.

The observed behaviours suggest that under thermal effect on the $SNPs^{FL}$/RF system, the RF fluorescence emission does not undergo major changes, thus no thermal degradation of its electronic structure in the excited state takes place. The findings are important regarding $SNPs^{FL}$/ RF containing drugs which would require thermal treatment for such a purpose like controlled release.

On the Trp band, fluorescence emission spectrum of $SNPs^{FL}$/RF system shows an emission maximum at 343 nm, 3 nm blue-shifted compared with $SNPs^{FL}$, Fig. 10a. Comparing both systems, two iso-emissive points at 358 / 387 nm are observed. Under temperature effect, a similar shape is observed with the maximum emission wavelength unchanged at 343 nm, Fig. 10c. A shoulder at ~ 390 nm, attributed to RF fluorescence traces, as a result of H-bonds between RF carbonyl group and hydroxyl Trp at SNPs surface, decreased as temperature increases. No significant changes, in the fluorescence excitation spectra, regarding the absorbance intensity, shifts and shape for both $SNPs^{FL}$ and $SNPs^{FL}$/RF systems are noticed, Figs. b and d.

Regarding 3D-excitation-emission matrix measurements, it appears from Fig. 11 that RF maintains its high fluorescence 367, 449 nm/528 nm bands in the presence of $SNPs^{FL}$, but Trp is quenched by it, as the intensity of the band at 286, 308 nm/ 350 nm decreases in respect to the data above described for $SNPs^{FL}$.

From lifetime measurements, RF in aqueous medium has a mono-exponential decay with a 4.74 ns lifetime, but a second, shorter, component of 2.62 ns appears in the presence of SNPs [31]. Data in Table 2 indicate that at the RF interaction with $SNPs^{FL}$, the decays are three exponential, with a new short lifetime of 0.21 ns being present. The emission decays with the corresponding fits of $SNPs^{FL}$ / RF system on the RF band are depicted in Fig. 12.

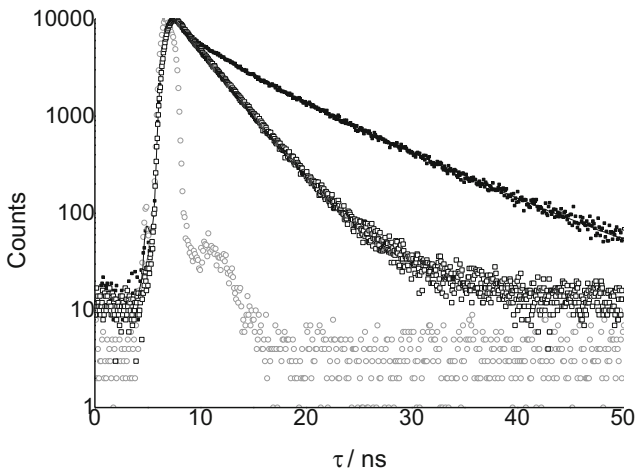

Fig. 12 Fluorescence decays of $SNPs^{FL}$ / RF at 450 (hollow squares) and 530 nm (full squares) emission wavelength

Conclusions

Fluorescent silver nano-structured system, has been obtained by chemical reduction of aqueous $AgNO_3$ solution by Tryptophan (Trp) using Dextran 70 as stabilizing agent ($SNPs^{FL}$). The formed fluorescent nanostructures are stable, multi-twined nanoparticle, with the size within 15–40 nm. The surface plasmon resonance peak of $SNPs^{FL}$ shows maximum absorption at 463 nm, the fluorescence emission at 346 nm with the fluorescence quantum yield, Φ = 0.034 and the integrated fluorescence lifetime, $<\tau>$ = 1.82 nm. Also, an increase in Trp surface hydrophobicity with λ_{em} = 328 nm, occurs.

Riboflavin fluorescence behaviour in the RF/$SNPs^{FL}$ system, does not undergo major structural changes; RF maintains its high fluorescence at λ_{em} = 530 nm with its reduction on the NPs surface.

The results support the ideas that $SNPs^{FL}$ would be stable in the pharmaceutical formulations and for using them as a

potential marker/emissive system to solve various biological barriers in humans, like drug release and protein containing Trp structure.

Acknowledgements This work was done within the research programme "Quantum Chemistry and Molecular Structure" of the Institute of Physical Chemistry "Ilie Murgulescu" of the Romanian Academy.

Compliance with Ethical Standards

Conflict of Interest None.

References

1. Roy K, Mao HQ, Huang SK, Leong KW (1999) Oral gene delivery with chitosan-DNA nanoparticles generates immunologic protection in a murine model of peanut allergy. Nat Med 5:387–391
2. Langer R (2001) Drug delivery: drugs on target. Science 293:58–59
3. De Jong WH, Borm PJA (2008) Drug delivery and nanoparticles: applications and hazards. Int J Nanomedicine 3:133–149
4. Li P, Li J, Wu C, Wu Q, Li J (2005) Synergistic antibacterial effects of β-lactam antibiotic combined with silver nanoparticles. Nanotechnology 16:1912–1917
5. Wong KKY, Liu X (2010) Silver nanoparticles–the real "silver bullet" in clinical medicine? Med Chem Commun 1:125–131
6. Jain P, Predeep T (2005) Potential of silver nanoparticles – coated polyurethane foam as an antibacterial water filter. Biotechnol Bioeng 90:59–63
7. Li Y, Leung P, Yao L, Song QW, Newton E (2006) Antimicrobial effect of surgical masks coated with nanoparticles. J Hosp Infec 62: 58–63
8. Shrivastava S, Bera T, Roy A, Sing G, Ramachandrarao P, Dash D (2007) Characterization of enhanced antibacterial effects of novel silver nanoparticles. Nanotechnology 18:1–9
9. Duran N, Marcato PD, De Conti R, Alves OL, Costa FTM, Brocchi M (2010) Potential use of silver nanoparticles on pathogenic bacteria, their toxicity and possible mechanism of action. J Braz Chem Soc 21:949–959
10. de Lima R, Seabra AB, Duran N (2012) Silver nanoparticles: a brief review of cytotoxicity and genotoxicity of chemically and biogenically synthesized nanoparticles. J Appl Toxicol 32:867–879
11. Rai M, Yadav A, Gade A (2009) Silver nanoparticles as a new generation of antimicrobials. Biotechnology Adv 27:76–83
12. Khodashenas B, Ghorbani HR (2015) Synthesis of silver nanoparticles with different shapes. Arab J Chem. https://doi.org/10.1016/j.arabjc.2014.12.014
13. Zhang A, Zhang J, Fang Y (2008) Photoluminescence from colloidal silver nanoparticles. J Lumin 128:1635–1640
14. Das R, Nath SS, Chakdar D, Gope G, Bhattacharjee R (2010) Synthesis of silver nanoparticles and their optical properties. J Exp Nanosci 5:357–362
15. Abdulah A, Annapoorni S (2005) Fluorescent silver nanoparticles via exploding wire technique. Prama J Phys 65:815–819
16. Zheng J, Dickson RM (2002) Individual water soluble dendrimer-encapsulated silver nanodot fluorescence. J Am Chem Soc 124: 13982–13983
17. Jian Z, Xiang Z, Yongchang W (2005) Electrochemical synthesis and fluorescence spectrum properties of silver nanospheres. Microelectron Eng 77:58–62
18. Ashenfelter BA, Desireddy A, Yan SH, Goodson IIIT, Bigioni TP (2015) Fluorescence from molecular silver nanoparticles. J Phys Chem C 119:20728–20734. https://doi.org/10.1021/acs.jpcc.5b05735
19. Jacob JA, Naumov S, Mukherjee T, Kapoor S (2011) Preparation, characterization, surface modification and redox reactions of silver nanoparticles in the presence of tryptophan. Colloid Surface B 87: 498–504
20. Parang Z, Keshavarz A, Farahi S, Elahi SM, Ghoranneviss M, Parhoodeh S (2012) Fluorescence emission spectra of silver and silver/cobalt nanoparticles. Sci Iran 19:943–947
21. Mane Gavade SJ, Nikam GH, Sabale SR, Tamhankar BV (2016) Green synthesis of fluorescent silver nanoparticles using acacia Nilotica gum extract for kinetic studies of 4-nitrophenol reduction. Mater Today – Proc 3:4109–4114
22. Ishida Y, Nakabayashi R, Corpuz RD, Yonezawa T (2017) Water-dispersible fluorescent silver nanoparticles via sputtering deposition over liquid polymer using a very short thiol ligand. Colloid Surfaces A 518:25–29
23. Jia K, Shou H, Wang P, Chen W, Liu X (2017) One-step synthesis of fluorescent silver nanoparticles with modulate emission wavelength using oligo–polyarylene ether nitrile as surface capping agent. J Mater Sci Mater Electron 28:16747–16754
24. Sing AK, Kanchanapally R, Fan Z, Senapati D, Rai PC (2012) Synthesis of highly fluorescent water-soluble silver nanoparticles for selective detection of Pb (II) at the parts per quadrillion (PPQ) level. Chem Commun 48:9047–9049
25. Zhou T, Rong M, Cai Z, Yang CJ, Chen X (2012) Sonochemical synthesis of highly fluorescent glutathione –stabilized ag nanoclusters and S^{2-} sensing. Nanoscale 4:4103–4106
26. Oliveira E, Santos HM, Garcia-Pardo J, Diniz M, Lorenzo J, Rodriguez-Gonzalez B, Capelo JL, Lodeiro C (2013) Synthesis of functionalized of fluorescent silver nanoparticles and their toxicological effect in aquatic environments (goldfish) and HepG2 cells. Front Chem 1:1–11
27. Shmarakov IO, Mukha IP, Karavan VK, Chunikhin OY, Marchenko MM, Smirnova NP, Eremenko AM (2014) Tryptophan–assisted synthesis reduces bimetallic gold/silver nanoparticles cytotoxicity and improves biological activity. Nanobiomedicine 1:6. https://doi.org/10.5772/59684
28. Navarro JR, Werts MH (2013) Resonant light scattering spectroscopy of gold, silver and gold-silver alloy nanoparticles and optical detection in microfluidic channels. Analyst 138:583–592
29. Chen RF (1967) Fluorescence quntum yields of tryptophan and tyrosine. Anal Lett 1:35–42
30. Voicescu M, Ionescu S, Angelescu DG (2012) Spectroscopic and course-grained simulation studies of the BSA and HSA protein adsorption on silver nanoparticles. J Nanopart Res 14(1174)
31. Voicescu M, Angelescu G, Ionescu S, Teodorescu VS (2013) Spectroscopic analysis of the roboflavin-serum albumins interaction on silver nanoparticles. J Nanopart Res 15(1555)
32. Voicescu M, Heinrich M, Hellwig P (2009) Steady-state and time-resolved fluorescence analysis on tyrosine - histidine model compounds. J Fluoresc 19:257–266
33. Voicescu M, El Khoury Y, Martel D, Heinrich M, Hellwig P (2009) Spectroscopic analysis of tyrosine derivatives: on the role of the tyrosine-histidine covalent linkage in cytochrome c oxidase. J Phys Chem B 113:13429–13436
34. Lakowicz JR (2000) On spectral relaxation in proteins. Photochem Photobiol 72:421–437
35. Albani JR (2014) Origin of tryptophan fluorescence lifetimes part 1. Fluorescence lifetimes origin of tryptophan free in solution. J Fluoresc 24:93–104
36. Miura R (2001) Versatility and specificity in flavoenzymes: control mechanisms of flavin reactivity. Chem Rec 1:183–194
37. Veselkov AN, Evstigneev MP, Rozvadovkaya AQ et al (2005) 1H RMN analysis of the complex formationof aromatic molecules of

antibiotic and vitamin in aqueous solution: heteroassociation of actinomycin D and flavin mononucleotide. Biophysics 50:20–27
38. Ramu A, Mehta MM, Liu J, Turyan I, Aleksic A (2000) The riboflavin mediated photooxidation of dexorubicin. Cancer Chemother Pharmacol 46:449–458
39. Evstigneev MP, Evstigneev VP, Hemander Santiago AA et al (2006) Effect of mixture of caffeine and nicotinamide on the solubility of vitamin B2 in aqueous solution. Eur J Pharm Sci 28:59–66
40. Voicescu M, Ionita G, Constantinescu T, Vasilescu M (2006) The oxidative activity of riboflavin studied by luminescence methods: the effect of cysteine, arginine, lysine and histidine amino acids. Rev Roum Chim 51:683–690
41. Edwards AM, Silva E, Jofre B et al (1994) Visible light effects on tumoral cells in a culture medium enriched with tryptophan and riboflavin. Photochem Photobiol 24:179–186
42. Voicescu M, Ionescu S, Manoiu VS, Anastasescu M, Craciunescu O, Moldovan L (2019) Synthesis and biophysical characteristics of riboflavin/HSA protein system on silver *nanoparticles*. Mat Sci Eng C 96:30–40